Reconstruction of turbulence characteristics from fluctuation reflectometry measurements in the nonlinear regime

P Tretinnikov, E Gusakov, Stéphane Heuraux

Reconstruction of turbulence characteristics from fluctuation reflectometry measurements in the nonlinear regime

P. Tretinnikov,[1,a)] E. Gusakov,[1] and S. Heuraux[2]

AFFILIATIONS

[1]Ioffe Institute, 194021 Saint-Petersburg, Russia
[2]Institut Jean Lamour, 50400 Nancy, France

[a)]Corresponding Author : tretinnikov@mail.ioffe.ru

ABSTRACT

The nonlinear theory of radial correlation reflectometry (RCR) predicts that the cross correlation function of a signal follows a Gaussian distribution with a cutoff separation, where the correlation length is determined by both the turbulence amplitude and its radial correlation length. In contrast, phase spectrum analysis provides information solely on the turbulence amplitude. This work describes the possibility of applying both signal analysis methods and demonstrates that turbulence amplitude and radial correlation length can be simultaneously measured using RCR diagnostics in the nonlinear regime.

https://doi.org/10.1063/5.0204394

I. INTRODUCTION

The radial correlation reflectometry is a widely used technique proposed to diagnose plasma turbulence in fusion machines. Initially, it was believed that probing plasma with multiple frequencies could determine the turbulence radial correlation length locally, simply from the difference in the cutoff positions where the correlation of the signals disappears. However, it was discovered that this naive approach is not always correct, leading to overestimation of the correlation length in the linear scattering regime[1,2] and underestimation in the nonlinear regime typical for large devices. This was demonstrated in the nonlinear theory of radial correlation reflectometry (RCR) in both 1D[3] and 2D[4] models and confirmed by numerical analysis in the 1D case.[5] According to the developed models, in the case of strong turbulence, the signal's spatial correlation length depends on both the turbulence radial correlation length and its amplitude, thus rendering it unhelpful for determining either of them.

Another method of analyzing reflectometry signals was developed to extract information on the turbulence spectrum and its amplitude.[6] This approach relies on the relationship between the radial wavenumber spectrum of density fluctuations and the phase fluctuation wavenumber spectrum of a reflectometer signal, established through a transfer function under the Born approximation,[7,8] valid in cases of weak turbulence. Parceval's theorem is employed in this method to locally recover the density fluctuation level and, consequently, the density fluctuation profile. It has been demonstrated that reconstructing the wavenumber spectrum is not feasible when the Born approximation is violated. However, it was observed that the turbulence amplitude can still be determined using Parceval's theorem.[9] This phenomenon was noted in 1D RCR simulations, where the turbulence amplitude was significant enough to break the Born approximation but still within limits where RCR remains within a moderately nonlinear regime.[9] The non-linear regime has been characterized in Ref. 10, demonstrating a reduction of the probing volume above a threshold in turbulence level and diffuse behavior of the probing wave scattering. At the same time, it exhibits the role of the wave resonance in turbulent plasma in maintaining, on average, the electromagnetic flux until the non-linear threshold[10] is reached.[11] This work tests the validity of phase variation spectrum analysis, originally developed for linear RCR regimes, in the nonlinear regime.

Hypothetically, the two methods can be combined to obtain information on both the turbulence amplitude and its radial correlation length under conditions where the nonlinear regime of RCR occurs. However, this concept has not been put into practice yet. This study aims to demonstrate and verify the feasibility of simultaneously utilizing the two methods of RCR signal interpretation as well as to evaluate the applicable domain for these techniques in intermediate turbulence levels encountered in actual fusion plasma devices.

II. REVIEW OF THE INTERPRETATIVE MODELS OF THE RADIAL CORRELATION REFLECTOMETRY

We will first discuss the two analytical interpretative models of RCR. We assume a slab geometry, which is typically adequate for characterizing microwave beam propagation in large machines. Cartesian coordinates are selected as follows: the x-axis denotes the direction of plasma inhomogeneity, with a probing ordinary mode polarization beam launched along this axis; the z-axis represents the direction of the external magnetic field; and the y-axis is perpendicular to both x and z, typically treated as the poloidal coordinate. We will consider 1D wave equation, assuming that the probing beam is wide, and also due to the lack of a 2D interpretative model for analyzing the spectrum of signal phase perturbations. In this model, the wave equation for the O-mode is as follows:

$$\left[\frac{\partial^2}{\partial x^2}+\frac{\omega^2}{c^2}\left(1-\frac{\omega_{pe}^2(x)}{\omega^2}-\frac{\delta n(x)}{n_c}\right)\right]_E=0, \tag{1}$$

where E represents the electric field amplitude (**E** is directed along the z-axis for O-mode polarization), ω_{pe} denotes the electron plasma frequency, n_c corresponds to the critical density value for a given probing frequency ω, and δn represents the turbulent density perturbation. The critical density determines a cutoff position x_c. The O-mode wave number k is given by the expression

$$k^2(x,\omega)=\frac{\omega^2-\omega_{pe}^2(x)}{c^2}. \tag{2}$$

The reflected electric field at the receiver E_r appears as follows:

$$E_r(\omega)=E_i e^{i\varphi_r(\omega)}, \tag{3}$$

where E_i represents the probing wave electric field amplitude and $\varphi_r=\varphi_0+\delta_\varphi$ denotes the reflected field phase. This phase consists of two components: φ_0, which is the phase associated with the wave propagation in the background plasma, and δ_φ, the phase perturbation caused by plasma turbulence.

One of the assumptions in the RCR interpretative models is a single cutoff position x_c for a probing frequency ω. It can be showed that this assumption is valid for

$$\frac{|\delta n|}{n_c}\ll\frac{l_{cx}}{x_c}, \tag{4}$$

where l_{cx} represents the radial correlation length of the turbulence. Additionally, the frozen turbulence approximation is employed in reflectometry analysis. This assumption entails that the characteristic variation time of turbulence is significantly longer than the time it takes for the probing wave to propagate. This condition typically holds true in reflectometry experiments. Both of these criteria are presumed to be met for both RCR interpretative models, which are further discussed in the text. Also long wavelength of the turbulence is assumed $l_{cx}\gg\lambda$, with λ being the probing wave wavelength. This criterion is necessary for applying the Wentzel–Kramers–Brillouin (WKB) description. Nevertheless, it is not always the case in a real experiment. Numerical simulation in this study demonstrates sensitivity of the interpretative models accuracy to this criterion.

A. Phase spectrum analysis

In the WKB approach, the phase variation linked to the density fluctuations δn can be expressed as a function of the cutoff position x_c,

$$\delta\varphi=-\frac{\omega}{c}\int_0^{x_c}\frac{dx'}{\sqrt{1-\frac{x'}{x_c}}}\frac{\delta n(x')}{n_c}. \tag{5}$$

A frequency sweep is employed to measure $\delta\varphi(x_c)$ across a range of cutoffs. Assuming that the main contribution comes from the cutoff layer, the phase variation wave number (q_x) Fourier transform $\delta\varphi_{q_x}$ in a RCR experiment can provide information about the turbulence amplitude. This is due to the relationship between the Fourier transform of the phase variation and the Fourier transform of the turbulence, which is as follows:

$$\langle|\delta\varphi_{q_x}|^2\rangle_N=\pi\frac{\omega^2}{c^2}\frac{x_c}{n_c^2}\frac{1}{|q_x|}\langle|n_{q_x}|^2\rangle_N, \tag{6}$$

where $\langle\ldots\rangle_N$ refers to the statistical average over N samples of the frequency ramp. This relation between the turbulence and phase perturbation spectra was initially derived under the Born approximation in Ref. 7 and further analyzed in detail in Ref. 9. It was demonstrated that even when the Born approximation is violated and the turbulence spectrum cannot be reconstructed, the turbulence amplitude can still be determined. This phenomenon was observed in 1D RCR simulations, where the turbulence amplitude was sufficiently large to break the Born approximation, yet not large enough to classify the RCR as deeply embedded in the nonlinear regime.

A set of N frequency sweep samples is required for the statistical analysis procedure. Two assumptions regarding the acquisition time are implicit in this technique of reflected wave phase analysis. The first assumption of independent samples implies that the correlation time of density fluctuations must be shorter than the time between two consecutive sweeps. For micro-turbulence measurements, this condition is met for repetition rates higher than 100 kHz, as the correlation of micro-turbulence typically lasts around 10 μs in tokamak plasmas. The second assumption of stationary plasma requires that the averaged plasma parameters, particularly the density profile, remain constant during the acquisition time of the N sweeps. These conditions can be reached experimentally by setting the duration of a frequency ramp to 1 μs and the time delay between two ramps greater than the correlation time.[12] When these criteria are satisfied, the root mean square (RMS) amplitude of turbulence (essentially its profile) can be evaluated from the measurements of reflected signal phase. It is also worth noting that this RCR analysis was described in a 1D model;[9] as of now, there is no 2D theory for phase perturbation analysis. To address 2D effects, numerical simulations are also conducted in this study.

B. Cross correlation function analysis in nonlinear regime of reflectometry

The cross correlation function (CCF) of the signal, corresponding to two probing frequencies ω_i and ω_j so the two cutoff positions x_{ci} and x_{cj}, is given by the following expression:

$$CCF(x_{ci}-x_{cj})=\frac{\langle\left(E_r(\omega_i)-\langle E_r(\omega_i)\rangle\right)\left(E_r^*(\omega_j)-\langle E_r^*(\omega_j)\rangle\right)\rangle}{\sqrt{\langle\left|\left(E_r(\omega_i)-\langle E_r(\omega_i)\rangle\right)\right|^2\rangle\langle\left|\left(E_r(\omega_j)-\langle E_r(\omega_j)\rangle\right)\right|^2\rangle}}. \tag{7}$$

The nonlinear theory makes use of the high phase variation due to the turbulence,

$$\langle \delta\varphi^2 \rangle \geqslant 1, \tag{8}$$

this is in contrast to the criterion set by the Born approximation. When the condition Eq. (8) (what we consider as the nonlinear regime criterion) is met, according to the theory,[3,4] the probing wave line extinction is observed $\langle E_r \rangle \propto e^{-\langle \delta\varphi^2 \rangle/2}$, and the RCR CCF takes on a relatively simple form,

$$CCF(x_{ci} - x_{cj}) = e^{i\left(\varphi_0(\omega_i) - \varphi_0(\omega_j)\right)} e^{-\frac{(x_{ci}-x_{cj})^2}{l_{ceff}^2}}, \tag{9}$$

where l_{ceff} represents the effective correlation length of the signal, which is determined by the following expression:

$$l_{ceff} = \left(\frac{\omega^2 x_c}{4c^2} \frac{\delta\tilde{n}^2}{n_c^2} \int dq_x |q_x| \tilde{n}^2_{q_x} \right)^{-1/2}, \tag{10}$$

where δn^{RMS} denotes the RMS amplitude of the turbulence and $\tilde{n}^2_{q_x}$ represents the turbulence spectrum. They are defined as follows:

$$\langle \delta n(x') \delta n(x'') \rangle = \left(\delta n^{RMS}\right)^2 \left((x' + x'')/2\right) \int \frac{dq_x}{2\pi} \tilde{n}^2_{q_x} e^{iq_x(x'-x'')}. \tag{11}$$

In the case of a Gaussian turbulence spectrum, characterized by the turbulence radial correlation length l_{cx} and given by the expression

$$\tilde{n}^2_{q_x} = \sqrt{\pi} l_{cx} e^{-\frac{l_{cx}^2 q_x^2}{4}}, \tag{12}$$

the effective RCR correlation length is given by

$$l_{ceff} = \pi^{-1/4} \frac{c}{\omega} \frac{n_c}{\delta n^{RMS}} \sqrt{\frac{l_{cx}}{x_c}}. \tag{13}$$

As shown in Refs. 3 and 4 in the case of an arbitrary turbulence spectrum, the RCR signals' CCF is also Gaussian in the nonlinear regime, though the numerical coefficient in dependence Eq. (13) may vary. From expression Eq. (13), it follows that measuring the *CCF* in the nonlinear regime of radial correlation reflectometry provides information on combinations of the turbulence amplitude δn^{RMS} and its radial correlation length l_{cx}. When the turbulence amplitude is known, the radial correlation length can be determined.

It is worth noting that the analysis of the signal cross correlation function in the nonlinear regime is conducted here within the framework of the 1D reflectometry model [considering the 1D wave equation as in Eq. (1)]. According to Ref. 4, when an emitter and receiver are situated sufficiently close, the analytical analysis of the 2D cross correlation function yields the same expressions as those in the 1D model. This analytical prediction is also verified numerically in the present study.

III. NUMERICAL SIMULATION OF RCR

The two techniques of the radial correlation reflectometry signal analysis were briefly outlined earlier. The phase perturbation spectrum analysis is not applicable for the turbulence wave number spectrum reconstruction when the Born approximation is violated; however, the turbulence amplitude can still be determined using Parceval's theorem. This observation was made in 1D RCR simulations, where the turbulence amplitude exceeded the threshold to break the Born approximation but remained within the moderately nonlinear regime.[9]

In this section, we numerically test the possibility of evaluating turbulence amplitude in the strongly nonlinear regime of RCR through 2D simulations. If this approach proves effective well beyond the Born approximation, the phase perturbation spectrum could offer insights into plasma turbulence amplitude in the nonlinear regime of radial correlation reflectometry. Consequently, assuming knowledge of the turbulence amplitude, the signal cross correlation function would then describe the radial correlation length of the turbulence. To assess the feasibility of simultaneously extracting information about both turbulence amplitude and its radial correlation length in an RCR experiment, numerical simulations of the RCR experiment were conducted.

The simulations were performed in the 2D geometry by the full-wave code IPF-FD3D.[13] In the simulations, a linear density profile within the slab 2D model was employed, and the radiating and receiving antennas are considered the same (no poloidal separation), producing Gaussian radiation pattern of the size ρ for the electric field. In the plasma parameters in the range of those encountered in experiments,

$$n(x) = n_0 \frac{x}{L} \tag{14}$$

with $L = 16.2$ cm and the density amplitude at $x = L$ $n_0 = 1 \times 10^{14}$ cm^{-3}, the simulations were conducted using a probing frequency range $f \in \{50 : 80\}$ GHz with a frequency step $\Delta f = 100$ MHz. This frequency range corresponds to a set of the cutoff positions ranging from $x_{c_{min}} = 4.9$ cm at the lower probing frequency to $x_{c_{max}} = 12.4$ cm at the upper one. The probing beam width was set to $\rho = 2$ cm in all simulations, except for one case where the influence of 2D geometry on RCR simulation results was investigated. In this case, a probing beam width of $\rho = 5$ cm was also tested.

In the simulations, homogeneous turbulence was set as input, with its constant RMS amplitude relative level, defined as

$$A = \frac{\delta n^{RMS}}{n(x_{c_{max}})}. \tag{15}$$

The isotropic Gaussian turbulence spectrum is employed in most simulations, spanning regimes with different correlation lengths $l_c = 1$ cm and $l_c = 3$ cm. The selection of the Gaussian spectrum facilitates clear control over turbulence parameters, helping in the comparison of numerical results with analytical predictions. The Gaussian turbulence spectrum Eq. (12) in the 2D model specifies the turbulence cross correlation function,

$$CCF_{\delta n}(x, y) = e^{-\frac{x^2+y^2}{l_c^2}}. \tag{16}$$

A simulation incorporating a realistic turbulence spectrum, built from experimental measurements, was also implemented. In this realistic scenario, the turbulence is assumed to be isotropic in 2D space, and its correlation length is defined as

$$l_c = \frac{1}{\sqrt{\pi}} \int dx CCF_{\delta n}(x, 0), \tag{17}$$

where the turbulence cross correlation function $CCF_{\delta n}$ is computed using the averaging procedure Eq. (11). The turbulence was generated as a sum of spatial harmonics with its spectral weight $\tilde{n}_{q_\perp}$ and a random phase $\phi_{k,l}$, and this is a standard approach often used for

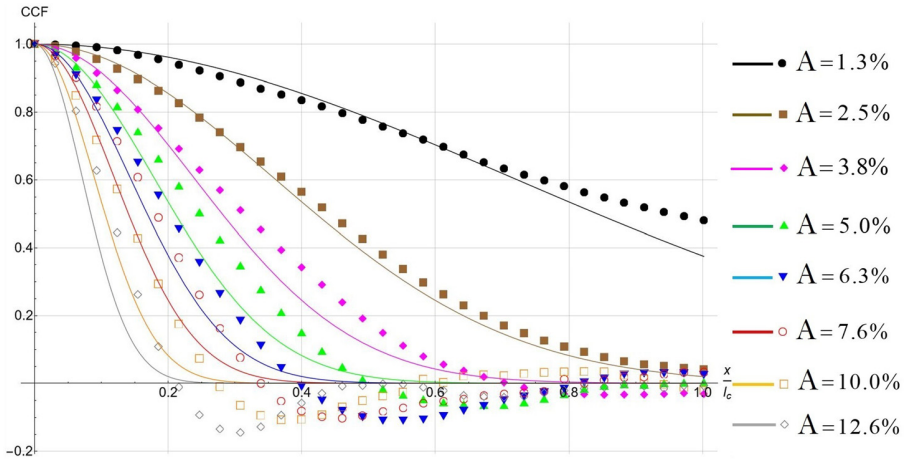

FIG. 1. *CCF* for the different turbulence amplitudes *A*. The solid curves represent the analytical cross correlation function, while the dotted curves depict the numerical results. The turbulence spectrum is Gaussian with the radial correlation length $l_c = 1$ cm, and the probing beam width ρ is set to 2 cm.

modeling the turbulence, which allows us to control the turbulence characteristics accurately,

$$\delta n(x,y) = \delta n^{RMS} \left(\frac{1}{2} \sum_{k,l} \tilde{n}^2_{q_\perp} \right)^{-1/2} \sum_{k,l} \tilde{n}_{q_\perp} \cos\left[q_k x + q_l y + \phi_{k,l} \right], \tag{18}$$

where $q_{k,l}$ are the discrete wavenumbers, for the Gaussian spectrum $\tilde{n}^2_{q_\perp} = \tilde{n}^2_{q_x} \tilde{n}^2_{q_y}$ (12). The simulations are conducted for different turbulence amplitudes and different turbulence spectra, and the results of the cross correlation function and the phase spectrum analysis are averaged over 1000 random turbulence realizations.

To facilitate the comparison between analytics and numerical modeling results, the cross correlation function Eq. (9) can be reduced to the following expression:

$$CCF(x_{ci} - x_{cj}) = e^{-\frac{(x_{ci} - x_{cj})^2}{l^2_{ceff}}}. \tag{19}$$

The unperturbed phase $\varphi_0(\omega)$, associated with the wave propagation in plasma, can be excluded from the registered signal. Thus, the simulated cross correlation function can be fitted with a Gaussian function to determine the effective correlation length l_{ceff}. Consequently, assuming the turbulence amplitude is known, the radial correlation length l_c of the turbulence can be determined. The reference point for constructing the cross correlation function is $x_{c_{max}}$ so the cross correlation function *CCF* is presented as a function of $CCF(x_{c_{max}} - x)$ in all figures presented throughout this paper.

A. Study on the beam width dependencies at fixed correlation length

The initial set of radial correlation reflectometry 2D simulations is conducted within the regime characterized by a Gaussian turbulence spectrum with a correlation length $l_c = 1$ cm, covering different turbulence amplitudes *A* ranging from 1.3% to 12.6%. The outcomes of the numerical evaluation of the signal cross correlation function are compared to the predictions of the analytical model, as illustrated in Fig. 1. By fitting the numerical *CCF* with a Gaussian function using the least squares method, the effective correlation length l_{ceff} is determined. Its dependence on the average phase variation squared is illustrated in Fig. 2. Assuming that the turbulence amplitude is known, the radial correlation length l_c can be found using Eq. (13). The numerically obtained radial correlation length is depicted in Fig. 3 for the simulated turbulence scenarios. It should be noted that the agreement between the analytical l_{ceff} and the numerically evaluated effective correlation lengths is relatively good (see Fig. 2), whereas the discrepancy for the radial correlation length l_c is much more pronounced (Fig. 3). This is due to the fact that $l_c \propto l^2_{ceff}$ Eq. (13).

There are two applicability criteria of the non-linear radial correlation reflectometry theory, which describes the signal cross correlation function. The first criterion is the strong modulation of the phase perturbations Eq. (10), which means that the turbulence amplitude *A* is assumed to be sufficiently high. The second criterion is related to the RCR model with a single cutoff Eq. (4), which limits maximal turbulence amplitude. The first point on Fig. 2 demonstrates that the average

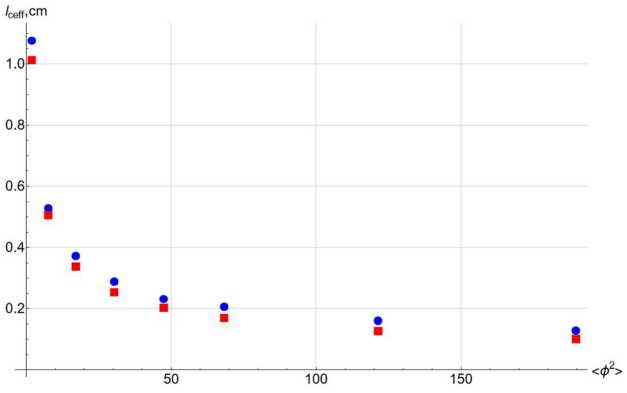

FIG. 2. The signal correlation length l_{ceff} vs the signal average phase variation squared, the different points correspond to the different turbulence amplitudes, and the turbulence amplitudes set is shown in Fig. 1. The blue circles represent the numerically evaluated l_{ceff}, and the red squares stand for the analytical values. The turbulence spectrum is Gaussian with $l_c = l$ cm and the probing beam width $\rho = 2$ cm.

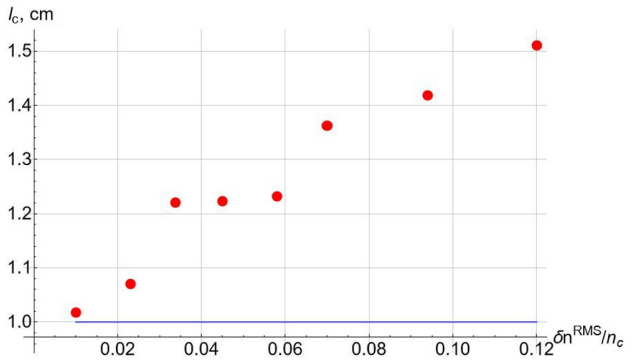

FIG. 3. The turbulence radial correlation length l_c evaluated numerically (red dot) vs the turbulence amplitude. The solid line is the analytical value of the turbulence correlation length l_c in the tested turbulence regime. The turbulence spectrum is Gaussian with $l_c = 1$ cm and the probing beam width $\rho = 2$ cm.

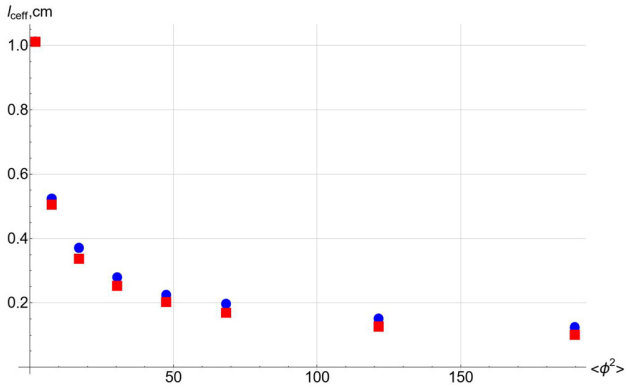

FIG. 5. The effective correlation length l_{ceff} vs the average phase variation squared, the different points correspond to the different tested turbulence amplitudes, and the corresponding turbulence amplitudes set is shown in Fig. 4. The blue circles represent the numerically evaluated l_{ceff}, and the red squares stand for the analytical values. The turbulence spectrum is Gaussian with $l_c = 1$ cm and the probing beam width $\rho = 5$ cm.

phase variation is approximately 1 for the turbulence amplitude $A = 1.3\%$, which represents the boundary of applicability for criterion Eq. (10). All the other points, corresponding to higher turbulence amplitude values, satisfy the strong phase modulation regime. It is also evident from Fig. 2 that in the strong phase modulation regime, the relation $l_{ceff} \ll l_c$ holds, which was utilized in the CCF nonlinear theory. Within the framework of the simulation model of the radial correlation reflectometry $\frac{l_c}{x_{c_{max}}} \approx 0.08$, thus, the boundary of applicability criterion for a single cutoff existence Eq. (4) is approximately $A = 8\%$. Therefore, the simulated turbulence amplitude set that roughly satisfies both criteria is as follows:

$$A \in \{2.5, 3.8, 5.0, 6.3\}\%. \tag{20}$$

This amplitude range corresponds to the points from the second to fifth on Figs. 2 and 3. The relative error of the radial correlation length l_c obtained in the turbulence amplitude range Eq. (20) is within 23%. The upper limit of the turbulence amplitude for the theory applicability explains the increase in discrepancy clearly observed from the sixth point onward in Fig. 3.

The next set of the numerical simulations was conducted using the same Gaussian turbulence spectrum with $l_c = 1$ cm and the same range of the tested turbulence amplitudes as it is specified in Fig. 1, but with a wider probing beam width $\rho = 5$ cm. Increasing the probing beam width brings the radial correlation reflectometry experiment closer to the 1D model. As stated in Sec. II B, the 1D and 2D models of the RCR in the nonlinear regime yield the same expression for the cross correlation function. The 1D nonlinear RCR theory was validated through 1D numerical simulations in Ref. 5; in this work, the comparison of 2D RCR numerical simulations with the 2D theory is performed first. Additionally, the analytical analysis of the phase perturbations spectrum was considered within the framework of 1D geometry.[9] Therefore, the importance of 2D effects for this analysis needs to be evaluated.

The results of the *CCF* numerical evaluation in the simulations with the different turbulence amplitudes (ranging from $A = 1.3\%$ to $A = 12.6\%$) are depicted in Fig. 4. The effective correlation length,

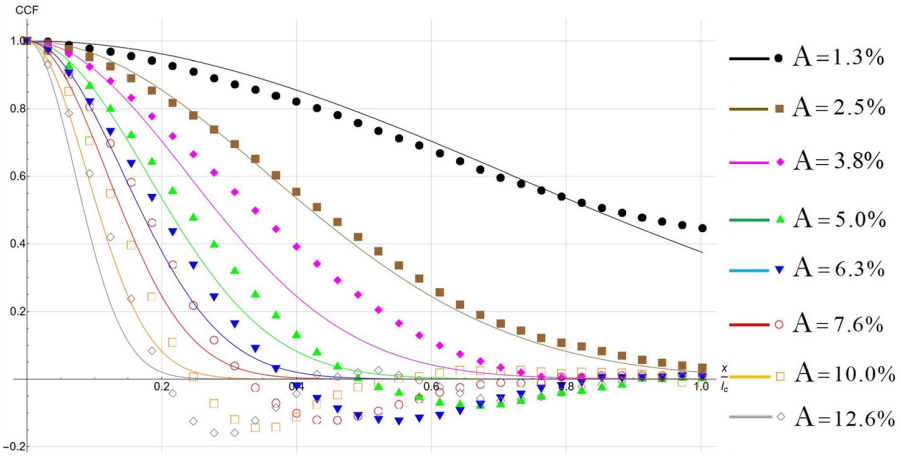

FIG. 4. *CCF* for the different turbulence amplitudes *A*, the analytical cross correlation function is represented by the solid curves, and the dotted curves demonstrate the numerical results. The turbulence spectrum is Gaussian with $l_c = 1$ cm and the probing beam width $\rho = 5$ cm.

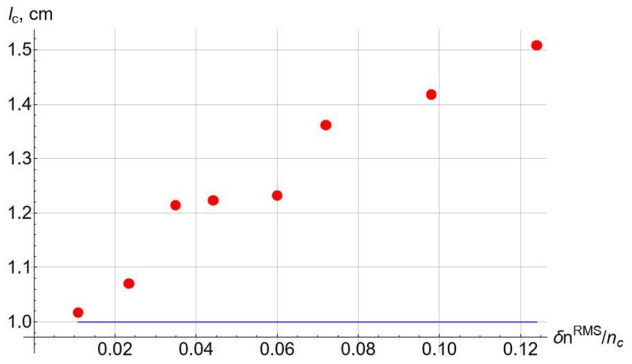

FIG. 6. The turbulence radial correlation length l_c as a function of the turbulence amplitude. The solid line is the tested value of the turbulence radial correlation length l_c. The turbulence spectrum is Gaussian with $l_c = l$ cm and the probing beam width $\rho = 5$ cm.

l_{ceff}, evaluated from fitting the simulated cross correlation function is depicted in Fig. 5. Finally, the turbulence radial correlation length l_c, determined from the evaluated effective correlation length l_{ceff}, is shown in Fig. 6. The applicability conditions in the simulations with a wider probing beam width remain the same as in the first set of the simulations with $\rho = 2$ cm so the analytical analysis is applicable for the same range of tested turbulence amplitudes Eq. (20). Comparing the results of the simulations with the different probing beam widths ($\rho = 2$ cm and $\rho = 5$ cm), one can observe that the signal cross correlation function *CCF*, demonstrated in Figs. 1 and 4, is almost the same in both numerical experiments. Consequently, there is minimal difference in the evaluated radial correlation length l_c depicted in Figs. 3 and 6. Therefore, we can conclude that the 2D theory of radial correlation reflectometry in the nonlinear regime[4] has been verified using the simulations.

B. Study on correlation length dependencies at fixed beam width

The next set of numerical simulations for radial correlation reflectometry is conducted in the regime with a Gaussian turbulence spectrum with a higher radial correlation length $l_c = 3$ cm. Increasing the turbulence radial correlation length allows for an extension of the turbulence amplitude range where the nonlinear RCR theory is applicable, Eq. (4). The *CCF* for different turbulence amplitudes is illustrated in Fig. 7. The effective correlation length l_{ceff} and the radial correlation length of the turbulence l_c, obtained from the evaluated value l_{ceff}, are demonstrated in Figs. 8 and 9, respectively. According to the simulated RCR model, $\frac{l_c}{x_{cmax}} \approx 0.24$, then the turbulence amplitude limit, restricting the applicability of the non-linear RCR theory, Eq. (4), is about $A \approx 24\%$. It should also be noted that even for the first point on Fig. 8, corresponding to the turbulence amplitude $A = 1.3\%$ and the average phase modulation squared $\langle \delta\varphi^2 \rangle \approx 2.5$, the signal correlation length l_{ceff} is approximately two times smaller than the turbulence correlation length l_c, indicating that the RCR is almost in the nonlinear regime. Thus, all the simulated regimes with different turbulence amplitudes can be described within the framework of the nonlinear theory of radial correlation reflectometry.

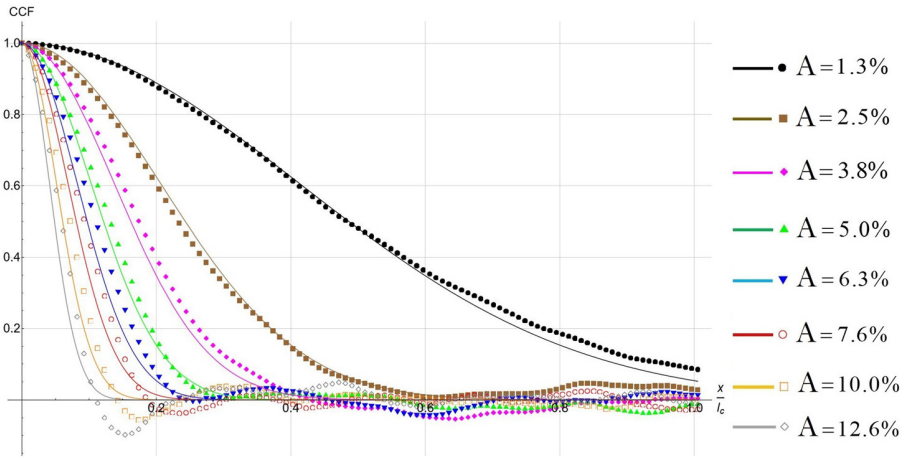

FIG. 8. The signal correlation length l_{ceff} vs the average phase variation squared, and the different points correspond to the different turbulence amplitudes. The blue circles represent the results of the *CCF* fitting by the Gaussian function of l_{ceff}, and the red squares stand for the analytical values. The turbulence spectrum is Gaussian with $l_c = 3$ cm, and the probing beam width $\rho = 2$ cm.

FIG. 7. *CCF* for the different turbulence amplitudes *A*, the analytical cross correlation function is represented by the solid curves, and the dotted curves stand for the numerical results. The turbulence spectrum is Gaussian with $l_c = 3$ cm, and the probing beam width $\rho = 2$ cm.

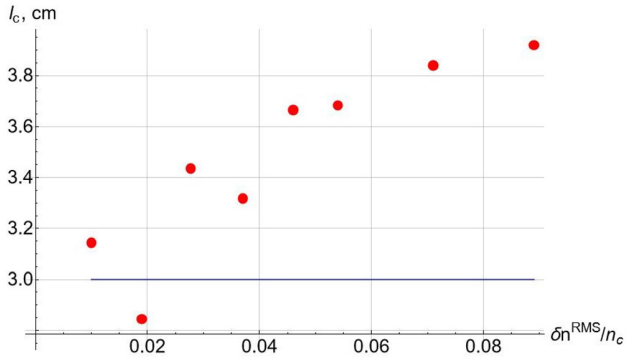

FIG. 9. The turbulence radial correlation length l_c evaluated numerically vs the turbulence amplitude. The solid line is the value of the turbulence correlation length l_c used in simulations. The turbulence spectrum is Gaussian with $l_c = 3$ cm, and the probing beam width $\rho = 2$ cm.

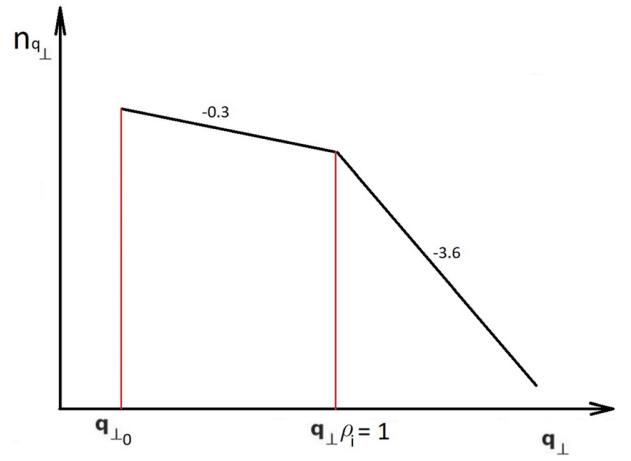

FIG. 10. The turbulence spectrum adapted from the experimental measurements at ASDEX Upgrade. The model spectrum is in logarithmic scale, and the spectrum is cut at $q_{\perp 0}$.

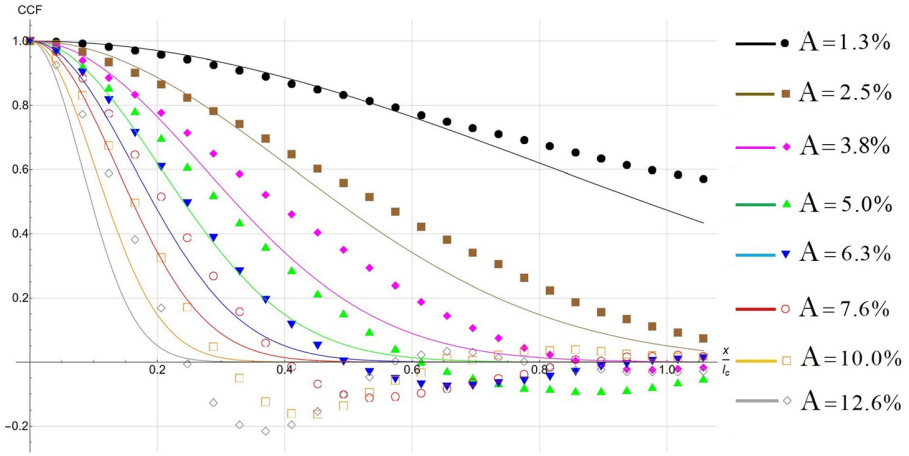

FIG. 11. *CCF* for the different turbulence amplitudes *A*, the analytical cross correlation function is represented by the solid curves, and the dotted curves stand for the numerical results. The turbulence spectrum is adapted from the experimental measurements at ASDEX Upgrade, and the probing beam width $\rho = 2$ cm.

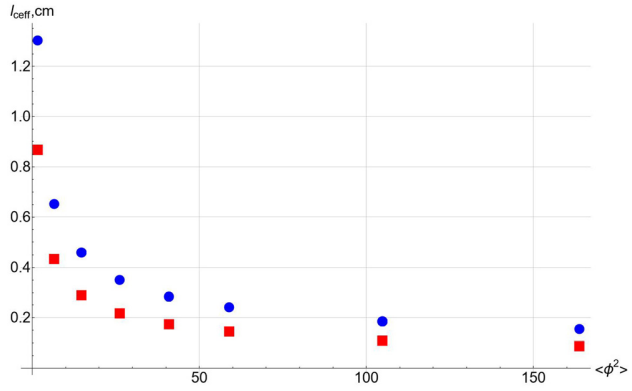

FIG. 12. The signal correlation length l_{ceff} vs the average phase variation squared, the different points correspond to the different turbulence amplitudes, and the turbulence amplitudes set is shown in Fig. 11. The blue circles represent the numerically evaluated l_{ceff}, and the red squares stand for the analytical values. The turbulence spectrum is adapted from the experimental measurements at ASDEX Upgrade, $l_c \approx 0.75$ cm, the probing beam width $\rho = 2$ cm.

C. Dependencies on the turbulent spectrum shape close to the experiment

The analogous simulations of RCR described earlier were conducted using the same model but with a turbulence spectrum generated from the experimental measurements at ASDEX Upgrade.[14] The turbulence spectrum $n_{q_\perp}$ is illustrated in a logarithmic scale in Fig. 10, and the spectrum is cut at $n_{q_{\perp 0}} = \frac{2\pi}{2a}$, where a represents the minor radius, ρ_i denotes the ion Larmor radius on Fig. 10, and the used parameters are $a = 200$ cm and $\rho_i = 0.3$ cm. The radial correlation length of the turbulence l_c, corresponding to the realistic turbulence spectrum and given by the definition in Eq. (17), is approximately 0.75 cm.

The cross correlation function evaluated for the turbulence regime with the experimental spectrum $n_{q_\perp}$ is depicted in Fig. 11 for the different turbulence amplitudes A. The effective correlation length l_{ceff}, defined from fitting the simulated *CCF*, is illustrated in Fig. 12. To obtain the turbulence radial correlation length l_c from l_{ceff}, the relation

Eq. (13) is used, though strictly speaking, it was derived for the Gaussian turbulence spectrum. The effective correlation length l_{ceff} in the case of an arbitrary turbulence spectrum is given by the expression Eq. (10). However, to obtain the turbulence radial correlation length l_c, the normalized turbulence spectrum $\tilde{n}^2_{q_x}$ must be described with a single parameter l_c. Since the turbulence spectrum in the considered model is described with two factors, which describe the wave number spectrum behavior before the knee position $q_\perp \rho_i = 1$ and after it (factors −0.3 and −3.6 in Fig. 10), and it also depends on the ion temperature and the tokamak size a, characterizing of the spectrum with a single parameter l_c is not possible. Therefore, the approximation based on the Gaussian turbulence spectrum Eq. (13) is used for evaluating the turbulence radial correlation length l_c, and the results of its evaluation are demonstrated in Fig. 13. A significant discrepancy between the tested turbulence radial correlation length l_c and the numerically evaluated values is observed. The relative error ranges from about 25% at the low turbulence amplitude value up to about 75% for the highest tested turbulence level. A pronounce discrepancy is also observed for l_{ceff} in Fig. 12; the numerically evaluated values for l_{ceff} are also significantly larger than the theory predicts, Eq. (10). This deviation indicates that this discrepancy is not related to the Gaussian spectrum interpretative model used for l_c definition.

According to the applicability criteria of the RCR non-linear theory [Eqs. (8) and (4)], the first tested turbulence amplitude $A = 1.3\%$ corresponds to $\langle \delta\varphi^2 \rangle \approx 1.6$, indicating that reflectometry is not deep in the nonlinear regime. Criterion Eq. (4) also sets the upper limit for the turbulence amplitude. For $l_c \approx 0.75$ cm, the turbulence amplitude is restricted by the value $A \approx 6\%$ [this is the border of the applicability criterion Eq. (4); the tractable in terms of the theory turbulence amplitudes should be much smaller], which explains the growing variance between the simulated turbulence radial correlation length l_c and the evaluated values starting from the third point in Fig. 13. Nevertheless, even for smaller amplitudes A, the relative error for l_c is within 43%. This discrepancy can be associated with a relatively small turbulence correlation length $l_c = 0.75$ cm compared to the probing wavelength 0.46 cm for an average probing frequency of 65 GHz. It should be mentioned that the WKB approach used for the *CCF* analysis also works well only for turbulence components with long wavelength. This fact is consistent with the results of the *CCF* simulations in the tested turbulence regimes. Namely, the consistency (in terms of the relative match between the theory and simulations) is the best for the simulations with the Gaussian turbulence spectrum possessing $l_c = 3$ cm, and it is the worst for the simulations with the realistic turbulence spectrum with $l_c = 0.75$ cm.

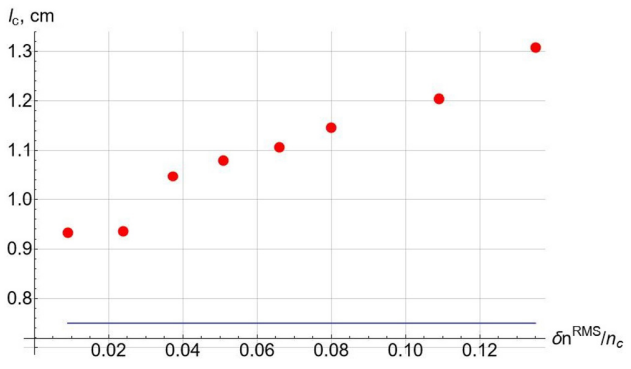

FIG. 13. The turbulence radial correlation length l_c evaluated numerically vs the turbulence amplitude. The solid line is the analytical value of the turbulence radial correlation length $l_c \approx 0.75$, evaluated according to Eq. (17) in the tested regime of the turbulence based on the experimental measurements. The probing beam width $\rho = 2$ cm.

D. Turbulence level evaluation

The turbulence amplitude can be defined from phase spectrum analysis using the relation Eq. (6) and Parseval's theorem, which is similar to previous method.[15] We utilized the homogeneous turbulence distribution in the described radial correlation reflectometry simulations. Hence, the RMS turbulence amplitude averaged within the radial window $R = x_{c_{max}} - x_{c_{min}}$ should coincide with the tested value δn^{RMS}. The tested analytical values of the turbulence amplitude, denoted as δn^{an}, are compared to the numerically evaluated values δn^{num} in Fig. 14. Figure 14 shows the evaluated turbulence amplitudes in all four tested regimes with different turbulence spectra: Gaussian spectra with $l_c = 1$ cm and $\rho = 2$ and 5 cm, Gaussian spectrum with $l_c = 3$ cm, and the spectrum measured in experiment with $l_c \approx 0.75$ cm. In the last two modes, the beam width $\rho = 2$ cm. The most significant discrepancy between δn^{num} and δn^{an} is observed in the regime with the high turbulence correlation length $l_c = 3$ cm. The reason for the pronounced variance is a relatively high contribution of the turbulence modes with small wave numbers q_x to the phase variation. This leads to an increase in contribution of small-angle scattering (this process can be significant in the nonlinear scattering regime[16]) to the phase variation, whereas the linear theory interprets $\delta\varphi$ as the Bragg backscattering;[9] the Bragg backscattering dominates in the cutoff layer where the WKB approximation is not applicable, and the condition $l_{cx} \gg \lambda$ is not met.[7] However, even in this case, the phase spectrum analysis provides the information about the turbulence amplitude with good accuracy, with a maximal relative error of about 30%.

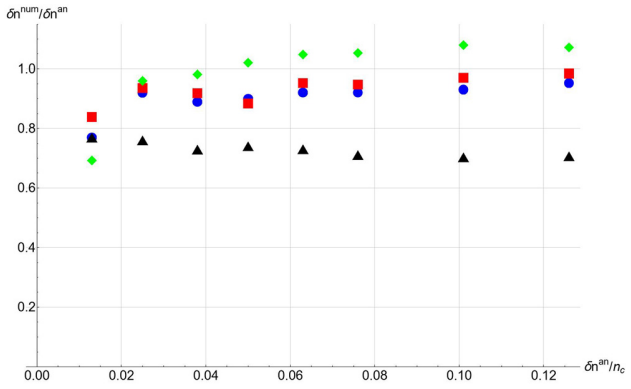

FIG. 14. The relation between the turbulence amplitudes evaluated from the phase perturbations spectrum analysis δn^{num} and the simulated amplitudes δn^{an} vs the relative tested turbulence amplitudes $A = \frac{\delta n^{an}}{n_c}$. The blue circles and red squares represent the results for the simulations with the Gaussian turbulence spectrum with $l_c = 1$ cm for $\rho = 2$ cm and $\rho = 5$ cm, respectively, the black triangles stand for the simulation with the Gaussian spectrum with $l_c = 3$ cm, and the green diamonds correspond to the simulations set with the experimental-like turbulence spectrum.

Also, it should be noted that the turbulence amplitude obtained from the phase spectrum analysis is almost the same in the two simulations with the Gaussian turbulence spectrum $l_c = 1$ cm and different probing beam widths $\rho = 2$ cm and $\rho = 5$ cm. This supports that the 2D effects do not play a significant role in the phase analysis technique, suggesting that the 1D description appears to be accurate.

IV. CONCLUSION

The phase perturbations spectrum analysis can provide information about turbulence amplitudes, and its analytical description was developed under the Born approximation in Refs. 6–9. In this paper, it is demonstrated that this method can be generalized far beyond the Born approximation criterion in the range of higher turbulence amplitudes. Then, we have a technique of the turbulence amplitude measurements in a RCR experiment for regimes with high turbulence amplitudes. This technique can be combined with the non-linear theory of the RCR, which describes the signal cross correlation function in the non-linear regime, Eqs. (10) and (13), and provides information about the combination of turbulence amplitude and its radial correlation length. The possibility of combining these two data analysis methods was verified by means of 2D full-wave numerical simulation in this work. It is demonstrated that turbulence amplitude and turbulence radial correlation length can be measured simultaneously in high-turbulence plasma scenario in an RCR experiment. A comparison with experiment would be useful as well; for this, it is necessary to compare the results of the proposed analysis with the results of other diagnostics measuring the amplitude of turbulence and its correlation length, if any.

The numerical simulations demonstrated that the turbulence amplitude δn^{RMS} can be determined from the phase perturbations spectrum analysis with a relative error ranging from few percents up to 30%, depending on the turbulence spectrum regime, as shown in Fig. 14. The effective correlation length l_{ceff} can be evaluated from fitting the cross correlation function, and the radial correlation length of the turbulence l_c can be defined according to the analytical relation Eq. (13). The simulations showed that l_c is normally overestimated for all the tested turbulence regimes, and the best agreement between the non-linear RCR theory and the results of the modeling is observed for the simulations with high radial correlation length $l_c = 3$ cm. In the simulated turbulence regimes with relatively low turbulence radial correlation lengths $l_c \approx 0.75$ cm (which can be considered as realistic), the error in the definition of l_c is significantly bigger (see Fig. 13). This is associated with the applicability limits of the non-linear RCR theory, mostly due to the single cutoff criterion when the radial correlation length is small enough according to Eq. (4), which can strongly restrict the range of suitable turbulence amplitudes for the non-linear RCR theory. To enhance the interpretative model of the *CCF* analysis in RCR experiments, a correction procedure should be implemented. Namely, the radial correlation length l_c, evaluated according to the described procedure of the *CCF* analysis, should be multiplied by a correcting factor. Assuming that the turbulence amplitude is known from the phase spectrum analysis, the correction factor can be estimated from simulations with the realistic turbulence spectrum, demonstrated in Fig. 13. This correction factor accounts for discrepancies between the evaluated l_c and the true turbulence radial correlation length. By applying this correction factor, the accuracy of the radial correlation length estimation in RCR experiments can be significantly improved.

Both techniques of RCR data analysis were previously tested by 1D numerical modeling. However, in this work, we conducted 2D simulations to test and verify these techniques for the first time. The results demonstrate that 2D geometrical effects do not significantly impact the data analysis. This finding aligns with the predictions from 2D analytical analysis of the RCR cross correlation function in the non-linear regime. While it was previously unclear how 2D effects might influence the phase perturbation spectrum analysis, our results confirm that they do not play a significant role in this context either. As to the influence of 3D effects, their role is not expected to be large because of strong elongation of the drift-wave turbulence in the magnetic field direction.

ACKNOWLEDGMENTS

Investigations presented in Secs. I, II, and IV of the paper were performed under support of the Ioffe institute state assignment FFUG-2024-0028 and the LUE program of the University of Lorraine, whereas the results presented in Sec. III were obtained in the framework of the state contract 0034-2021-0003.

Author Contributions

P. Tretinnikov: Formal analysis (lead); Investigation (lead); Methodology (equal); Software (lead); Validation (lead); Visualization (lead); Writing – original draft (lead). **E. Gusakov:** Conceptualization (lead); Formal analysis (lead); Methodology (lead); Project administration (lead); Supervision (lead); Validation (equal); Writing – original draft (equal). **S. Heuraux:** Conceptualization (lead); Data curation (equal); Formal analysis (lead); Methodology (lead); Supervision (lead); Validation (equal); Writing – original draft (equal).

DATA AVAILABILITY

The data that support the findings of this study are available within the article.

REFERENCES

[1] I. Hutchinson, Plasma Phys. Controlled Fusion **34**, 1225 (1992).
[2] E. Z. Gusakov and B. O. Yakovlev, Plasma Phys. Controlled Fusion **44**, 2525 (2002).
[3] E. Z. Gusakov and A. Y. Popov, Plasma Phys. Controlled Fusion **44**, 2327 (2002).
[4] E. Z. Gusakov and A. Y. Popov, Plasma Phys. Controlled Fusion **46**, 1393 (2004).
[5] G. Leclert, S. Heuraux, E. Z. Gusakov, A. Y. Popov, I. Boucher, and L. Vermare, Plasma Phys. Controlled Fusion **48**, 1389 (2006).
[6] S. Heuraux, S. Hacquin, F. da Silva, F. Clairet, R. Sabot, and G. Leclert, Rev. Sci. Instrum. **74**, 1501 (2003).
[7] C. Fanack, I. Boucher, F. Clairet, S. Heuraux, G. Leclert, and X. L. Zou, Plasma Phys. Controlled Fusion **38**, 1915 (1996).
[8] B. B. Afeyan, A. E. Chou, and B. I. Cohen, Plasma Phys. Controlled Fusion **37**, 315 (1995).
[9] L. Vermare, S. Heuraux, F. Clairet, G. Leclert, and F. D. Silva, Nucl. Fusion **46**, S743 (2006).
[10] E. Z. Gusakov, S. Heuraux, and A. Y. Popov, Plasma Phys. Controlled Fusion **51**, 065018 (2009).

[11]E. V. Sysoeva, E. Z. Gusakov, and S. Heuraux, Plasma Phys. Controlled Fusion **55**, 115001 (2013).
[12]F. Clairet, C. Bottereau, A. Medvedeva, D. Molina, G. D. Conway, A. Silva, U. Stroth, ASDEX Upgrade Team, Tore Supra Team, and EUROfusion MST1 Team, Rev. Sci. Instrum. **88**, 113506 (2017).
[13]C. Lechte, G. D. Conway, T. Görler, C. Tröster-Schmid, and the ASDEX Upgrade Team, Plasma Phys. Controlled Fusion **59**, 075006 (2017).
[14]T. Happel, T. Görler, P. Hennequin, C. Lechte, M. Bernert, G. D. Conway, S. J. Freethy, C. Honoré, J. R. Pinzón, U. Stroth *et al.*, Plasma Phys. Controlled Fusion **59**, 054009 (2017).
[15]E. Z. Gusakov, S. Heuraux, A. Yu Popov, and M. Schubert, Plasma Phys. Controlled Fusion **54**, 045008 (2012).
[16]E. Z. Gusakov, A. V. Surkov, and A. Y. Popov, Plasma Phys. Controlled Fusion **47**, 959–974 (2005).